

Multiphoton excited hemoglobin fluorescence and third harmonic generation for non-invasive microscopy of stored blood

ILYAS SAYTASHEV,¹ RACHEL GLENN,¹ GABRIELLE A. MURASHOVA,¹ SAM OSSEIRAN,^{2,3} DANA SPENCE,¹ CONOR L. EVANS,³ AND MARCOS DANTUS^{1,4,*}

¹Department of Chemistry, Michigan State University, 578 S Shaw Ln., East Lansing, MI 48824, USA

²Harvard-MIT Division of Health Sciences and Technology, 77 Massachusetts Avenue E25-519, Cambridge, MA 02139, USA

³Wellman Center for Photomedicine, Harvard Medical School, Massachusetts General Hospital, 149 13th Street, Charlestown, MA 02129, USA

⁴Department of Physics and Astronomy, Michigan State University, 567 Wilson Rd., East Lansing, MI 48824, USA

*dantus@msu.edu

Abstract: Red blood cells (RBC) in two-photon excited fluorescence (TPEF) microscopy usually appear as dark disks because of their low fluorescent signal. Here we use 15fs 800nm pulses for TPEF, 45fs 1060nm pulses for three-photon excited fluorescence, and third harmonic generation (THG) imaging. We find sufficient fluorescent signal that we attribute to hemoglobin fluorescence after comparing time and wavelength resolved spectra of other expected RBC endogenous fluorophores: NADH, FAD, biliverdin, and bilirubin. We find that both TPEF and THG microscopy can be used to examine erythrocyte morphology non-invasively without breaching a blood storage bag.

©2016 Optical Society of America

OCIS codes: (180.0180) Microscopy; (180.4315) Nonlinear Microscopy; (180.5810) Scanning microscopy.

References and links

1. R. Jimenez and F. E. Romesberg, "Excited state dynamics and heterogeneity of folded and unfolded states of cytochrome C," *J. Phys. Chem. B* **106**(35), 9172–9180 (2002).
2. W. Min, S. Lu, S. Chong, R. Roy, G. R. Holtom, and X. S. Xie, "Imaging chromophores with undetectable fluorescence by stimulated emission microscopy," *Nature* **461**(7267), 1105–1109 (2009).
3. W. Zheng, D. Li, Y. Zeng, Y. Luo, and J. Y. Qu, "Two-photon excited hemoglobin fluorescence," *Biomed. Opt. Express* **2**(1), 71–79 (2011).
4. E. Chaigneau, M. Oheim, E. Audinat, and S. Charpak, "Two-photon imaging of capillary blood flow in olfactory bulb glomeruli," *Proc. Natl. Acad. Sci. U.S.A.* **100**(22), 13081–13086 (2003).
5. C. Xu, W. Zipfel, J. B. Shear, R. M. Williams, and W. W. Webb, "Multiphoton fluorescence excitation: new spectral windows for biological nonlinear microscopy," *Proc. Natl. Acad. Sci. U.S.A.* **93**(20), 10763–10768 (1996).
6. P. Xi, Y. Andegeko, D. Pestov, V. V. Lovozoy, and M. Dantus, "Two-photon imaging using adaptive phase compensated ultrashort laser pulses," *J. Biomed. Opt.* **14**(1), 014002 (2009).
7. S. M. Frank, B. Abazyan, M. Ono, C. W. Hogue, D. B. Cohen, D. E. Berkowitz, P. M. Ness, and V. M. Barodka, "Decreased erythrocyte deformability after transfusion and the effects of erythrocyte storage duration," *Anesth. Analg.* **116**(5), 975–981 (2013).
8. O. N. Salaria, V. M. Barodka, C. W. Hogue, D. E. Berkowitz, P. M. Ness, J. O. Wasey, and S. M. Frank, "Impaired red blood cell deformability after transfusion of stored allogeneic blood but not autologous salvaged blood in cardiac surgery patients," *Anesth. Analg.* **118**(6), 1179–1187 (2014).
9. A. B. Zimrin and J. R. Hess, "Current issues relating to the transfusion of stored red blood cells," *Vox Sang.* **96**(2), 93–103 (2009).
10. G. Edgren, M. Kamper-Jørgensen, S. Eloranta, K. Rostgaard, B. Custer, H. Ullum, E. L. Murphy, M. P. Busch, M. Reilly, M. Melbye, H. Hjalgrim, and O. Nyrén, "Duration of red blood cell storage and survival of transfused patients (CME)," *Transfusion* **50**(6), 1185–1195 (2010).
11. S. D. Robinson, C. Janssen, E. B. Fretz, B. Berry, A. J. Chase, A. D. Siega, R. G. Carere, A. Fung, G. Simkus, W. P. Klinke, and J. D. Hilton, "Red blood cell storage duration and mortality in patients undergoing percutaneous coronary intervention," *Am. Heart J.* **159**(5), 876–881 (2010).

12. A. H. M. van Straten, M. A. Soliman Hamad, A. A. van Zundert, E. J. Martens, J. F. ter Woorst, A. M. de Wolf, and V. Scharnhorst, "Effect of duration of red blood cell storage on early and late mortality after coronary artery bypass grafting," *J. Thorac. Cardiovasc. Surg.* **141**(1), 231–237 (2011).
13. S. D. Shukla, R. Coleman, J. B. Finean, and R. H. Michell, "The use of phospholipase c to detect structural changes in the membranes of human erythrocytes aged by storage," *Biochim. Biophys. Acta* **512**(2), 341–349 (1978).
14. B. Blasi, A. D'Alessandro, N. Ramundo, and L. Zolla, "Red blood cell storage and cell morphology," *Transfus. Med.* **22**(2), 90–96 (2012).
15. I. Moon, F. Yi, Y. H. Lee, B. Javidi, D. Boss, and P. Marquet, "Automated quantitative analysis of 3D morphology and mean corpuscular hemoglobin in human red blood cells stored in different periods," *Opt. Express* **21**(25), 30947–30957 (2013).
16. D. Fu, T. Ye, T. E. Matthews, B. J. Chen, G. Yurtserver, and W. S. Warren, "High-resolution in vivo imaging of blood vessels without labeling," *Opt. Lett.* **32**(18), 2641–2643 (2007).
17. D. Li, W. Zheng, Y. Zeng, Y. Luo, and J. Y. Qu, "Two-photon excited hemoglobin fluorescence provides contrast mechanism for label-free imaging of microvasculature in vivo," *Opt. Lett.* **36**(6), 834–836 (2011).
18. R. D. Schaller, J. C. Johnson, and R. J. Saykally, "Nonlinear chemical imaging microscopy: near-field third harmonic generation imaging of human red blood cells," *Anal. Chem.* **72**(21), 5361–5364 (2000).
19. G. O. Clay, A. C. Millard, C. B. Schaffer, J. Aus-der-Au, P. S. Tsai, J. A. Squier, and D. Kleinfeld, "Spectroscopy of third-harmonic generation: evidence for resonances in model compounds and ligated hemoglobin," *J. Opt. Soc. Am. B* **23**(5), 932–950 (2006).
20. B. Nie, I. Saytashev, A. Chong, H. Liu, S. N. Arhipov, F. W. Wise, and M. Dantus, "Multimodal microscopy with sub-30 fs Yb fiber laser oscillator," *Biomed. Opt. Express* **3**(7), 1750–1756 (2012).
21. B. Nie, D. Pestov, F. W. Wise, and M. Dantus, "An ultrafast fiber laser with self-similar evolution in the gain segment," *Opt. Photonics News* **22**(12), 47 (2011).
22. S. Lu, W. Min, S. Chong, G. R. Holtom, and X. S. Xie, "Label-free imaging of heme proteins with two-photon excited photothermal lens microscopy," *Appl. Phys. Lett.* **96**(11), 113701 (2010).
23. J. A. Meyer, J. M. Froelich, G. E. Reid, W. K. Karunaratne, and D. M. Spence, "Metal-activated C-peptide Facilitates Glucose Clearance and the Release of a Nitric Oxide Stimulus via the GLUT1 Transporter," *Diabetologia* **51**(1), 175–182 (2007).
24. Y. Wang, A. Giebink, and D. M. Spence, "Microfluidic evaluation of red cells collected and stored in modified processing solutions used in blood banking," *Integr. Biol.* **6**(1), 65–75 (2014).
25. J. T. Dodge, C. Mitchell, and D. J. Hanahan, "The preparation and chemical characteristics of hemoglobin-free ghosts of human erythrocytes," *Arch. Biochem. Biophys.* **100**(1), 119–130 (1963).
26. R. Dasgupta, S. Ahlawat, R. S. Verma, A. Uppal, and P. K. Gupta, "Hemoglobin degradation in human erythrocytes with long-duration near-infrared laser exposure in Raman optical tweezers," *J. Biomed. Opt.* **15**(5), 055009 (2010).
27. J. P. Greer, D. A. Arber, B. Glader, A. F. List, R. T. Means, F. Paraskevas, and G. M. Rodgers, *Wintrobe's Clinical Hematology*, (Lippincott Williams & Wilkins, 2013), p. 3094.
28. K. Jaferzadeh and I. Moon, "Quantitative investigation of red blood cell three-dimensional geometric and chemical changes in the storage lesion using digital holographic microscopy," *J. Biomed. Opt.* **20**(11), 111218 (2015).
29. I. Moon, F. Yi, Y. H. Lee, B. Javidi, D. Boss, and P. Marquet, "Automated quantitative analysis of 3D morphology and mean corpuscular hemoglobin in human red blood cells stored in different periods," *Opt. Express* **21**(25), 30947–30957 (2013).
30. G. Brecher and M. Bessis, "Present status of spiculed red cells and their relationship to the discocyte-echinocyte transformation: a critical review," *Blood* **40**(3), 333–344 (1972).
31. B. F. Rodak, *Diagnostic Hematology* (Saunders, Philadelphia, 1995).
32. B. J. Bain, *Blood Cells: A Practical Guide*, 5 edition ed. (Wiley-Blackwell, Hoboken, NJ, 2015).
33. Y. Barad, H. Eisenberg, M. Horowitz, and Y. Silberberg, "Nonlinear scanning laser microscopy by third harmonic generation," *Appl. Phys. Lett.* **70**(8), 922–924 (1997).
34. D. Débarre, N. Olivier, and E. Beaurepaire, "Signal epidetection in third-harmonic generation microscopy of turbid media," *Opt. Express* **15**(14), 8913–8924 (2007).
35. Y. Zeng, B. Yan, Q. Sun, S. K. Teh, W. Zhang, Z. Wen, and J. Y. Qu, "Label-free in vivo imaging of human leukocytes using two-photon excited endogenous fluorescence," *J. Biomed. Opt.* **18**(4), 040504 (2013).
36. G. O. Clay, C. B. Schaffer, and D. Kleinfeld, "Large two-photon absorptivity of hemoglobin in the infrared range of 780–880 nm," *J. Chem. Phys.* **126**(2), 025102 (2007).
37. A. A. Rehms and P. R. Callis, "Two-photon fluorescence excitation spectra of aromatic amino acids," *Chem. Phys. Lett.* **208**(3–4), 276–282 (1993).
38. B. Kierdaszuk, I. Gryczynski, A. Modrak-Wojcik, A. Bzowska, D. Shugar, and J. R. Lakowicz, "Fluorescence of tyrosine and tryptophan in proteins using one- and two-photon excitation," *Photochem. Photobiol.* **61**(4), 319–324 (1995).
39. S. Yoshida, T. Iizuka, T. Nozawa, and M. Hatano, "Studies on the charge transfer band in high spin state of ferric myoglobin and hemoglobin by low temperature optical and magnetic circular dichroism spectroscopy," *Biochim. Biophys. Acta* **405**(1), 122–135 (1975).

40. L. M. Snyder, F. Garver, S. C. Liu, L. Leb, J. Trainor, and N. L. Fortier, "Demonstration of haemoglobin associated with isolated, purified spectrin from senescent human red cells," *Br. J. Haematol.* **61**(3), 415–419 (1985).
41. Q. Sun, W. Zheng, J. Wang, Y. Luo, and J. Y. Qu, "Mechanism of two-photon excited hemoglobin fluorescence emission," *J. Biomed. Opt.* **20**(10), 105014 (2015).
42. P. P. Ho and R. R. Alfano, "Optical Kerr Effect in Liquids," *Phys. Rev. A* **20**(5), 2170–2187 (1979).

1. Introduction

Two-photon excitation fluorescence (TPEF) imaging of unstained red blood cells (RBCs) for non-invasive label-free blood analysis and deformability has been deemed undetectable at 800nm [1–3]. This assessment is based upon the fact that spontaneous emission is dominated by fast non-radiative decay [1, 2]. RBCs exhibit strong absorption and are known to cast dark shadows in nonlinear fluorescence imaging of capillaries *in vivo* [4]. While increasing laser intensity may yield a fluorescence signal that is strong enough for label-free analysis, the high intensity would likely cause both linear and nonlinear photo-thermal damage to the RBCs, especially when using pulse widths greater than 150fs. TPEF intensity is highly dependent on the characteristics of the laser source, with shorter pulse durations leading to higher fluorescence emission yields [5, 6]. It follows that short pulse durations may lead to appropriately high levels of TPEF signal, while limiting nonlinear photo-thermal damage for optimal non-destructive imaging.

The long-term storage of RBCs leads to known changes in their health status. Current protocols call for the destruction of these stored blood components after 42 days, based on guidelines from the Committee for Standardization in Haematology [15]. As RBCs age, they lose the important flexibility and deformability that enables them to squeeze through small capillaries to deliver oxygen to tissue; this capability cannot be regained after the transfusion occurs [7, 8]. Indeed, the effects of older (>14 days) transfused blood on mortality have been the subject of numerous studies [9–12]. Recent work analyzing RBC cell membrane deformability before and three days following surgery found that storage times longer than three weeks led to irreversible damage to RBCs, which are then removed by the liver [7, 8]. If blood could be imaged quickly and non-invasively prior to transfusion, it may be possible to assess the health of RBCs and thus reduce the risk of postoperative complications. Similarly, in emergencies, it may be possible to find healthy RBCs in blood beyond the 42 days storage, thus extending the availability of limited blood supplies.

Non-invasive monitoring of RBC health via changes in cellular morphology can be accomplished, in principle, by imaging RBCs through the blood bag. Previous optical imaging studies of RBC morphology have required breaching the storage bag; these efforts, like those described above, found irreversible changes to the morphology with increasing storage duration [13–15]. Nonlinear optical imaging of RBCs has been accomplished via several different methods including two-photon absorption (TPA) [2, 16], TPEF [3, 17], and THG [18, 19]. For TPA imaging, an intensity modulated pump pulse train at 775nm and delayed probe at 650nm were employed based upon the different excited state dynamics of oxyhemoglobin and deoxyhemoglobin [16]. TPEF imaging has been accomplished via two-photon excitation of the Soret band in hemoglobin with ~250 fs pulses in the 600-750nm wavelength range [3] [17]. The fluorescence signal severely diminished when the excitation wavelength exceeded 750nm [3]. Spectroscopic measurements were made on a solution of stabilized human lyophilized ferrous hemoglobin powder. Imaging of fresh mice blood was accomplished with 600nm excitation wavelength [3], a wavelength that produced the strongest signal. Previous studies have shown that TPEF signal increases by decreasing pulse duration [5, 6]. This suggests that short < 20fs pulses at 800 nm might be useful for imaging RBCs by enhancing TPEF while keeping the number of laser photons (thermal energy) to a minimum. THG images of RBCs, on the other hand, have been efficiently generated by tuning the excitation wavelength to achieve resonant enhancement via the Soret band [18, 19].

We propose a method to image RBC morphology that does not require breaching the sterile environment of the blood storage bag. This consideration distinguishes the present study from prior work in that it provides a solid foundation for assessing RBC status non-destructively in a clinical setting. We explore TPEF and THG modalities and compare these different contrast mechanisms to determine guidelines for imaging RBCs in storage while maintaining sterility. Nonlinear imaging with pulses shorter than 50fs from a Yb-fiber laser produce bright THG images of tissues [20]; here, we used a short-pulse Yb-fiber oscillator [21] and a short-pulse Ti:Sapphire laser to image RBCs. Additional time and frequency resolved measurements were carried out in order to assign the emission signals.

2. Materials and methods

Two different lasers were used for this work. We used an 86 MHz repetition rate Ti:Sapphire laser (KM labs, Boulder, CO), with an external pulse shaper (MIIPS Box 640, Biophotonic Solutions Inc., East Lansing, MI), producing sub-15fs pulses; and a 42 MHz repetition rate Yb-fiber laser with a built-in pulse shaper (MIIPS HD, Biophotonic Solutions Inc., East Lansing, MI) [21] producing sub-45 fs pulses. The laser output is scanned by a pair of galvanometer mirrors (QuantumDrive 1500, Nutfield Technology, Inc., Hudson, NH) as illustrated in Fig. 1. Dispersion correction, including high-order terms accumulated in the beam path, was accomplished using multiphoton intrapulse interference phase scan (MIIPS) [6] using an ultra-thin BBO crystal located at the focal plane (Microscope Detection Unit, Biophotonic Solutions Inc., East Lansing, MI). For imaging we used a 40x water immersion objective with a working distance of 0.5mm (Zeiss LD-C APOCHROMAT 1.1 NA, Jena, Germany), mounted on a TE200 inverted microscope (Nikon, Tokyo, Japan), modified for multi-photon microscopy.

TPEF spectra and fluorescence-lifetime decay measurements were carried out in the epi direction using a 16 channel time-correlated single photon counting (TCSPC) system (SPC-830, Becker & Hickl GmbH, Berlin, Germany). Images were obtained in the epi direction using a photomultiplier tube (PMT) (HC20-05MOD, Hamamatsu, Japan) after de-scanning and separation of signals using a 635nm long-pass dichroic mirror (Di02-R635-25x36, Semrock Inc., NY) and a 680nm short-pass emission filter (ET680-SP-2P8, Chroma Technology Corp., VT). The microscope objective and filter combination in the epi direction resulted in poor THG detection efficiency at ~353nm.

In the forward direction, THG was collected by a 15x objective (ReflX for UV, NT59-886, NA 0.28, Edmund Optics Inc., NJ) using a 410nm short-pass filter (410SP, Chroma Technology Corp., VT). This filter prevents detection of three-photon excited fluorescence expected at ~480nm. The forward signal was detected by a different PMT detector (H10720-210, Hamamatsu, Japan). Signals were digitized by a PC data acquisition board for further image reconstruction. Ten to thirty 512x512 16-bit grayscale raw images were combined into a stack. An ImageJ (NIH, MD, USA) software function for averaging images in a stack was performed resulting in a single 16-bit grayscale image. Brightness and contrast levels were adjusted to increase the visibility of RBCs and the image was converted to 8-bit grayscale. False coloring from grayscale to shades of red was performed for Fig. 2 and 4(b). Images were cropped to exclude scanning aberrations at the edge of the field of view. No editing was performed within the images.

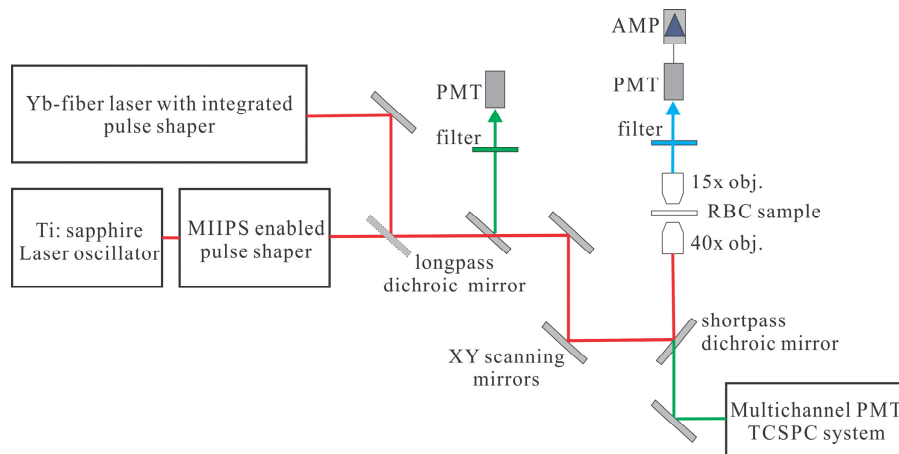


Fig. 1. Schematic diagram of the microscopy setup for multi-photon imaging using different lasers. Ti:Sapphire or Yb-fiber laser oscillators can be used one at a time.

A separate system was also used to measure the transient absorption (TA) properties of hemoglobin, which relies on the sequential stepwise absorption of two photons from the ground state to a final excited state via an intermediate excited state. TA measurements were obtained from both human hemoglobin (Sigma-Aldrich H7379, St. Louis, MO) and red blood cells obtained from mice in accordance with the Institutional Animal Care and Use Committee of the Massachusetts General Hospital (IACUC protocol #2016N000078). Imaging was performed with a tunable dual-output pulsed femtosecond laser source (Spectra-Physics Insight DeepSee, Santa Clara, CA), using the fixed 1040nm output as the pump beam and the tunable output set to 735nm as the probe beam. This configuration allows for the stepwise absorption of 1040nm and 735nm photons by hemoglobin, which roughly equates to the absorption of a single 430nm photon. Similar multiphoton-based absorption techniques have been used and validated in the past to visualize heme proteins, such as in the case of two-photon excited photothermal lens microscopy [22]. Intensity modulation of the 1040nm beam was achieved using an electro-optic modulator (Thorlabs EO-AM-R-20-C2, Newton, NJ) with 20 MHz modulation. Imaging was carried out on a modified confocal microscope (Olympus FV1000, Center Valley, PA) using a 1.20 NA 60x water immersion objective (Olympus UPLSAPO 60XW, Center Valley, PA). Forward detection was achieved using a photodiode coupled to a lock-in amplifier (APE Lock-in Amplifier, Berlin, Germany) placed downstream of a 710nm longpass filter (Chroma E710LP, Bellows Falls, VT) and a 950nm shortpass filter (Thorlabs FES0950, Newton, NJ). This configuration allows the transmission of the 735nm probe beam to the photodiode while blocking the 1040nm pump beam, where the lock-in amplifier can detect any intensity modulation transfer from the pump beam to the probe beam at the 20MHz modulation frequency. The output of the lock-in amplifier is then fed into an Olympus input-output box system and digitized for acquisition by the Olympus Fluoview confocal microscopy control software.

All procedures involving human subjects, including consent forms, were approved by the Biomedical and Health Institutional Review Board (BIRB) at Michigan State University. Whole blood was obtained from consented healthy human donors by venipuncture and collected into heparinized tubes [23]. Upon collection in a citrate phosphate dextrose buffer solution, the blood was immediately centrifuged for 10min at 500g and 4°C. The plasma and leukocytes were removed by filtration and the RBCs were added to an AS-1 storage solution. RBCs were subsequently diluted from ~70% to 0.4% in AS-1 solution for imaging. RBCs were introduced either in a chamber containing prepared RBCs or directly inside a sealed PVC blood storage bag (200 gauge PVC, 50µm thick film) (Uline, WI) - the same as used for commercial storage - and hermetically enclosed by thermal splicing [24].

Erythrocyte ghosts (the resulting RBC membrane with all other intracellular components removed) were prepared according to a wash protocol based on published work [25]. RBCs were suspended in PBS, and then washed 3x at 500g for 10 minutes with the supernatant aspirated off after each wash. Four 40 μ L aliquots of compact RBCs suspended in 1mL lysis buffer (described below) were then centrifuged at 22,000g for 15 minutes. After discarding the supernatant, the remaining membranes were washed in lysis buffer 3x at 22,000g for 5 minutes. Finally, the supernatant was discarded, and the lysates were pooled. Lysis buffer was prepared by mixing 10 mM Tris-HCl with 0.2 mM ethylenediaminetetraacetic acid (EDTA) at pH 7.2. The linear absorbance of erythrocyte ghosts was measured using a Unicam UV-2 spectrophotometer (ATi Unicam, Cambridge, UK) in a 1 mm quartz cuvette.

3. Results

3.1 TPEF microscopy imaging of RBCs on a coverslip and through PVC bag using Ti:Sapphire laser

TPEF images of human RBCs were obtained in the epi direction with the 800nm Ti:Sapphire laser as shown in Fig. 2 and through the PVC storage bag in Fig. 3. Individual RBCs and their central pallor can clearly be seen.

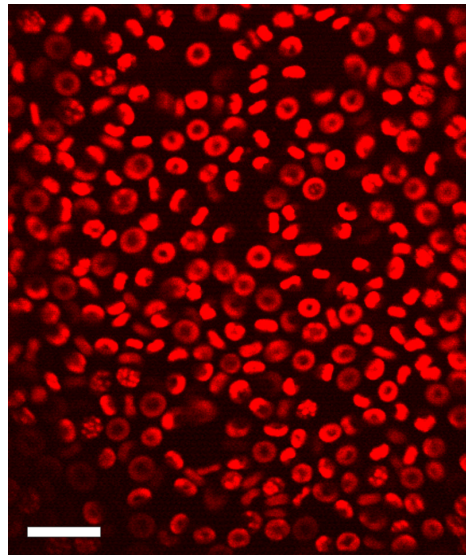


Fig. 2. TPEF image of unstained human RBCs on a coverslip imaged by 15fs pulses with 10mW average power from the Ti:Sapphire laser tuned to 800 nm. Scale bar is 20 μ m.

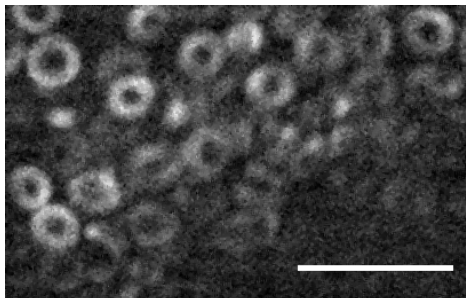


Fig. 3. TPEF image of RBCs detected through the PVC storage bag in the epi direction obtained with 10mW average power 15fs pulses from the Ti:Sapphire laser tuned to 800 nm. Scale bar is 20 μ m. Video of flowing RBCs ([Visualization 1](#)).

The possibility of photodamage was carefully considered. At lower excitation power (<5mW) the TPEF signals are very weak, but no signs of photodamage were observed in RBC appearance after > 2min of exposure. With an increase of excitation power to 10mW or 22mW using 800nm or 1060nm lasers, respectively, we observed both cell shrinkage and an increase of the fluorescence signal after tens of seconds of exposure. Similar photodamage effects on RBCs have been reported during optical trapping of human erythrocytes [26].

RBC morphology can be clearly seen in Fig. 3 and is important for determination of hematologic diseases. In fact, many diseases have normal blood counts but abnormal membrane morphology [27]. Under normal circumstances, mature RBCs are round biconcave disc-shaped cells measuring 7-8 microns in diameter. Both THG and TPEF modalities allow measurements of the average cell diameter and thickness. From our results we obtain from TPEF a mean diameter and one standard deviation $6.9 \pm 0.5 \mu\text{m}$ and from THG a mean diameter of $8.1 \pm 0.5 \mu\text{m}$. We do not consider the different diameters to be significant given that these were two different blood samples. Taking into account a measured thickness of $2.2 \pm 0.2 \mu\text{m}$ we are able to estimate the mean volume at $82 \pm 11 \mu\text{m}^3$ and the surface area at $123 \pm 18 \mu\text{m}^2$. Previous studies using holographic microscopy of RBCs reported a variation of the diameter [28] ranging from $6\mu\text{m}$ - $7.8\mu\text{m}$, corpuscular volume [28, 29] ranging from 88 to 102 CV [μm^3], and surface area [29] ranging from 107 to 131 μm^2 with increasing storage times from 8 to 57 days.

It is well known that preparation of fresh blood between coverslips can affect RBC appearance, where they can become echinocytes (star shaped RBCs) [30]. Moreover, the blood collection tube is internally coated with EDTA. While its role is to prevent coagulation of collected blood, there is a possibility that echinocytosis may occur upon contact of RBCs with the EDTA coating [31]. In the blood storage bag, however, the concentration of EDTA is low enough that echinocytosis is not likely to occur [32]. Nevertheless, we expect that other morphological deformities such as elliptocytosis, cigar cells, schistocytosis, and sickle cells can indeed occur, and can be determined by non-destructive TPEF imaging.

3.2 THG microscopy imaging of RBCs on a coverslip and through PVC bag using Yb-fiber laser

THG microscopy does not require fluorescence from the molecule; THG signal generation only requires a change in the index of refraction at the focus [33]. While THG typically requires high peak intensities for imaging, this limitation is easily overcome by using shorter pulses and a lower average power. In Fig. 4, the images were generated with less than 8mW of average laser power at the objective focus. THG images of RBCs on a glass cover slip detected in the trans direction are shown in Fig. 4. Compared to TPEF, the RBC membrane boundaries are clearly seen on the THG image. The non-zero background in Fig. 4 is a direct result of the out-of-focus THG signal generated from the glass-liquid interface.

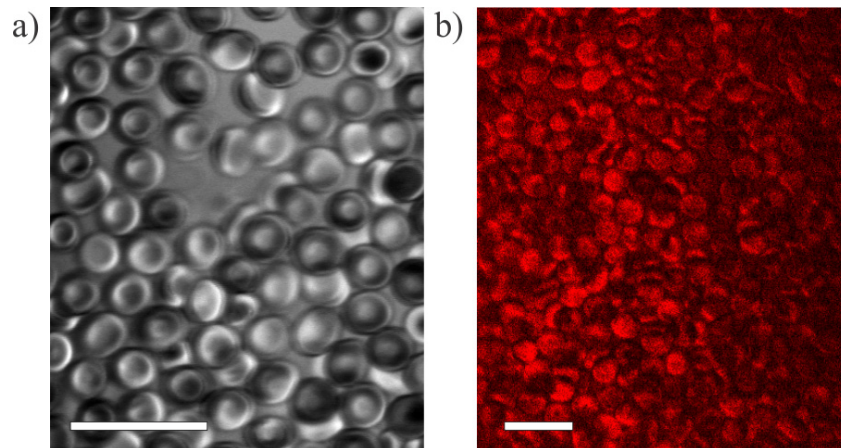


Fig. 4. THG microscopy imaging of human RBCs on the glass cover slip obtained using a 1060 nm Yb-fiber laser emitting 45fs pulses with 8mW average power. a) Static image; b) Video of flowing RBCs ([Visualization 2](#)). Scale bar is 20 μ m.

Precise morphology measurements such as RBC size can be performed with or without the blood bag. We used an Yb-fiber laser with a central wavelength of 1060nm and 45fs duration pulses to image RBCs through the PVC storage bag, as shown in Fig. 5. The nonlinear optical signal was detected in both trans and epi directions, as shown in Fig. 5(a) and Fig. 5(b), respectively. For the trans direction acquisition, images were obtained near the edge of the PVC storage bag where absorption of the THG signal was minimized. In the epi direction, on the other hand, imaging can be performed anywhere in the bag. There is a difference with the images taken in the epi and trans direction, which is due to the emission being directional and phase matching favoring trans detection. The dependence of epi versus trans detection of THG signal has been quantified, with trans detection being best for thin samples and epi detection being strongly favored for thick samples where the signal corresponds to backscatter [34]. The shape of RBCs can be clearly seen in both images. It is worth noting that the average excitation power was maintained below 20mW in order to avoid damaging the PVC bag, which occurs above 25mW.

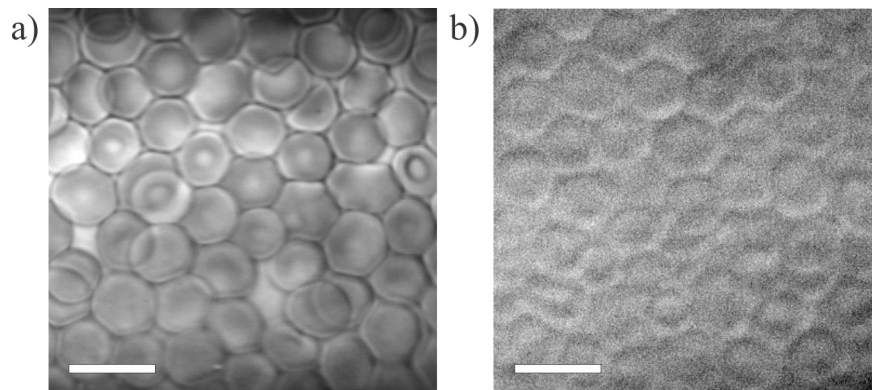


Fig. 5. THG images of RBCs detected through the PVC storage bag in trans direction (a) and in epi direction (b) excited by 7mW average power from an Yb-fiber laser. Scale bar is 10 μ m.

3.3 The source of fluorescence in RBCs

TPEF fluorescence from RBCs and erythrocyte ghosts has a broad emission spectrum from 400 to 570nm with a peak around 480nm that can be excited by two 800nm photons. This weak fluorescence emission from blood has been attributed to a number of sources in past

studies, including flavin-containing molecules such as flavin adenine dinucleotide (FAD) and riboflavin, nicotinamide adenine dinucleotide (NADH) [35], hemoglobin [3,36] and its fluorescent catabolites – biliverdin and bilirubin. Tryptophan, a common residue to most proteins, has an absorption band in the 260-290 nm range that can be reached via three-photon excitation by the Ti:Sapphire laser, but not the Yb-fiber [37]. Excitation produces a broad fluorescence centered at 340 nm that extends from 310 to 370nm. Fluorescence from RBCs was centered near 480nm. While it is possible that tryptophan was excited by the Ti:Sapphire laser, little or no fluorescence would be detected in our experiment given the 370nm long pass filter in our setup. The fluorescence lifetime reported for tryptophan in proteins shows a small amplitude ~ 0.2 for the 0.5ns component and the two equally weighted major components with ~ 2 ns and ~ 5 ns lifetime, respectively [38]. The difference in emission wavelength and fluorescence lifetime allows us to rule out tryptophan as the source of RBC signal.

We investigated the fluorescence lifetime following one- (Fig. 6(a)) and two-photon (Fig. 6(b)) excitation for RBCs, erythrocyte ghosts, NADH, biliverdin, bilirubin, riboflavin and hemoglobin; all in physiological salt solution (PSS) containing 4.7mM KCl, 2.0mM CaCl_2 , 1.2mM MgSO_4 , 140.5mM NaCl, 21.0mM Tris-hydroxymethyl aminomethane, 5.5mM glucose, and 5% bovine serum albumin at pH = 7.4; all reagents were from Sigma Aldrich. The TPEF lifetime decays were measured and compared with one-photon excited (355nm centered 12ps laser pulses) fluorescence lifetime decays for the same samples. Bilirubin, RBCs, and erythrocyte ghosts did not exhibit detectable fluorescence upon one-photon UV excitation and are thus not present in Fig. 6(a). Table 1 summarizes fluorescence lifetimes for one-photon excitation measurements, and Table 2 summarizes two-photon excitation fluorescence lifetimes obtained by fitting decay curves using single and double exponential decay models. The system response time for the two-photon excitation measurements is ~ 130 ps, while the system response time for the single-photon TCSPC setup is ~ 45 ps (full-width at half maximum). We confirmed the two-photon dependence of the Hb TPEF detected as a function of laser intensity (reported as average laser power), and show those results in Fig. 7. Note that previous studies measured a TPEF lifetime for Hb excited at 600nm to be 230ps, a value indistinguishable from their system response time [3], whereas we measured a lifetime of 280 ± 20 ps. One explanation for the difference in lifetime is the intersystem crossing [3] and charge transfer states near 630nm [39], these pathways are not accessible when exciting at longer wavelengths. The NADH lifetime is dependent upon solvent pH, and whether it is bound or unbound. Bound and free forms of NADH are known to have lifetimes [35] corresponding to 1-2 ns and 450-600ps, respectively. We measured free NADH and found its lifetime in the 450-600ps range. Bound NADH has a lifetime that is too long to correspond to the TPEF signal from RBCs.

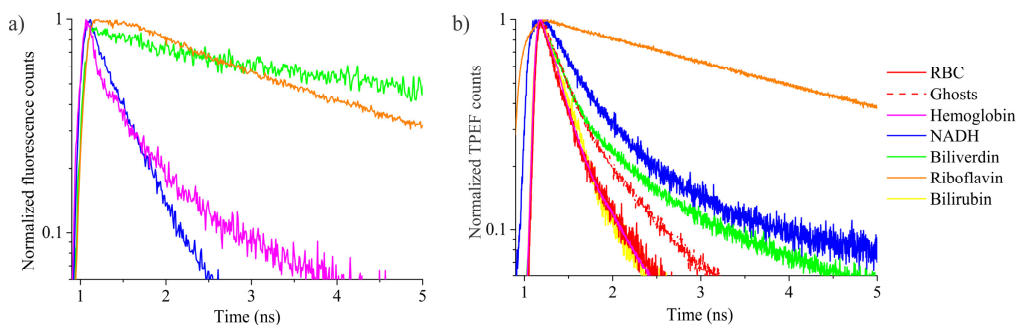


Fig. 6. (a) One-photon excitation (355nm, 12 ps) fluorescence decay curves of hemoglobin, NADH, biliverdin, and riboflavin compared to (b) TPEF (800nm, 15fs) decay curves for RBCs, their membranes and reagent-grade hemoglobin, biliverdin, bilirubin, riboflavin, and NADH.

Table 1. Fluorescence lifetime decays obtained from fitting one-photon excitation (355 nm) curves using single and double exponential models.

	A1, a.u.	τ_1 , ps	A2, a.u.	τ_2 , ps
20 μ M NADH in PSS	0.95 ± 0.04	412 ± 32	0.05 ± 0.04	$2416 \pm 400^*$
100 μ M NADH in PSS	0.99 ± 0.03	441 ± 29	0.013 ± 0.031	$3093 \pm 400^*$
50 μ M Riboflavin in PSS			1	3513 ± 9
2 g/L Hemoglobin in PSS	0.68 ± 0.04	223 ± 3	0.32 ± 0.04	1547 ± 15
1 mM Biliverdin in PSS			1	3272 ± 300

* less than 5% contribution for fitting

Table 2. Fluorescence lifetime decays obtained from fitting two-photon excitation (800 nm) curves using single and double exponential models.

	A1, a.u.	τ_1 , ps	A2, a.u.	τ_2 , ps
12 g/L Hemoglobin in PSS	0.88 ± 0.04	280 ± 20	0.12 ± 0.04	1260 ± 300
50 μ M NADH in PSS	0.85 ± 0.05	520 ± 40	0.16 ± 0.05	2140 ± 470
50 μ M Biliverdin in PSS	0.77 ± 0.02	320 ± 20	0.22 ± 0.02	2180 ± 140
50 μ M Bilirubin in PSS	0.98 ± 0.01	330 ± 10	0.02 ± 0.01	3700 ± 1500
50 μ M Riboflavin in PSS			1	4000 ± 50
Ghosts in PSS	0.75 ± 0.07	320 ± 40	0.25 ± 0.07	1340 ± 250
RBCs in PSS	0.83 ± 0.06	260 ± 30	0.18 ± 0.06	1170 ± 280

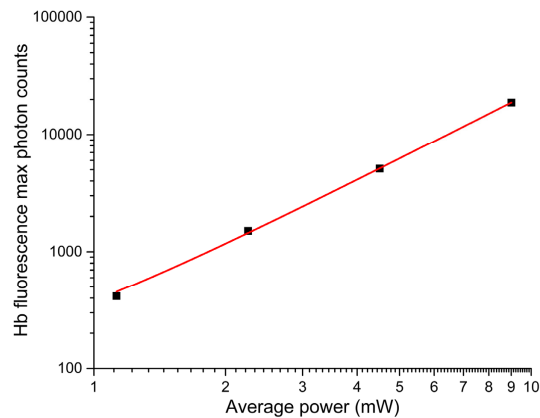


Fig. 7. Hemoglobin fluorescence signal versus average excitation power from Ti:Sapphire laser (14 fs pulse duration FWHM) plotted in a logarithmic scale. The experimental points are fit by a linear function with slope equal to 1.89 ± 0.03 , which is consistent with two-photon excited fluorescence.

TPEF emission spectra of RBCs, their membranes and commercially obtained fluorophores are shown in Fig. 8(a). To measure quantitatively the similarity between TPEF spectra, we calculated the Pearson correlation coefficients between the fluorescence spectrum of RBCs and that of other samples, as summarized in Table 3. Both bilirubin and riboflavin's weak Pearson correlation coefficients of 0.552 and 0.208, respectively, suggest that they are not responsible for RBC fluorescence. Furthermore, riboflavin was omitted from the comparative plot of TPEF peak wavelength vs. fluorescence lifetime (Fig. 8(b)), because its lifetime is over an order of magnitude longer than that of RBCs and ghosts. We therefore

conclude that the observed TPEF emission from RBCs and ghosts indeed originates from hemoglobin.

Table 3. Pearson correlation coefficients of TPEF spectra

RBC	Ghosts	Hemoglobin	NADH	Biliverdin	Bilirubin	Riboflavin
1.000	0.995	0.975	0.939	0.883	0.552	0.208

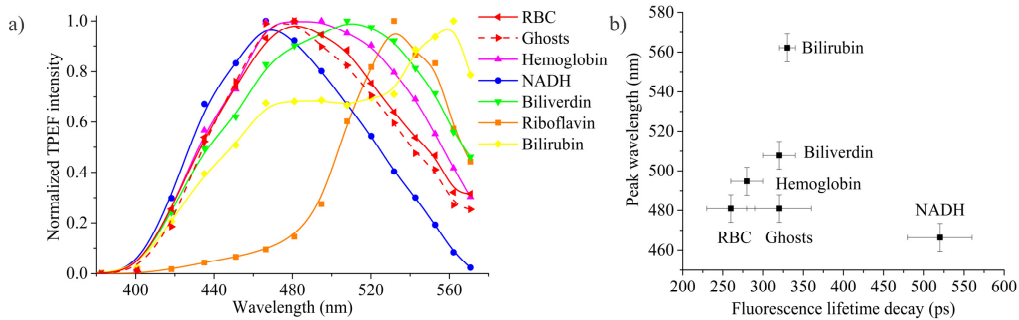


Fig. 8. (a) TPEF (800nm, 15 fs) emission spectra for RBCs, erythrocyte ghosts and reagent-grade fluorophores. (b) TPEF peak wavelength vs decay lifetimes for RBCs, their membranes and reagent-grade hemoglobin, biliverdin, bilirubin, and NADH.

It is well known that RBCs are densely packed with large amounts of hemoglobin. Hemoglobin is also bound to the membrane, as has been determined after several washes [40]. The absorption spectrum of hemoglobin originates from heme, having an intense Soret or B-band (~400-430 nm, depending on oxidation state) and weak transition to the Q-band (~550nm). It is known that the fluorescence emission of hemoglobin is undetectable with one-photon excitation; however TPEF imaging of hemoglobin has recently been demonstrated using two-photon excitation wavelengths ranging from 550nm to 750nm [41]. TPEF of hemoglobin excited at 800nm has not been reported in any prior work, despite hemoglobin's large two-photon absorption at longer wavelengths, with a maximum around 825nm [36].

Further confirmation of the participation of hemoglobin was obtained by comparing transient absorption decay curves for pure hemoglobin and purified RBCs in Fig. 9(a). In these experiments, we monitor transmission of 735 nm photons as a function of time following excitation with 1040nm photons. Absorption at 1040 nm is likely associated with the absorption of oxyhemoglobin at that wavelength. The similarity between the two suggests that the fluorescent signal from RBCs is the result of an excited state of hemoglobin, as opposed to other potential fluorophores. Background signal from the PBS solution appeared strictly when the two pulse trains were overlapped, likely due to the optical Kerr effect from the water solvent [42]. To first approximation, we assumed that hemoglobin was contained only within the volume of the RBC and not the membrane. Washing of the ghost cells was done to remove all hemoglobin, and we expected to find no more TPEF signal. We found that after three washes, the signal from hemoglobin remained constant, indicating that some of the hemoglobin was bound to the membrane and could not be removed. The inset in Fig. 9(b) tracks absorption at 414nm with increasing washes and shows that a certain percentage of hemoglobin remained. Previous methods with subsequent washing of RBCs also found a small percentage of hemoglobin in the membrane that cannot be removed via washing [40].

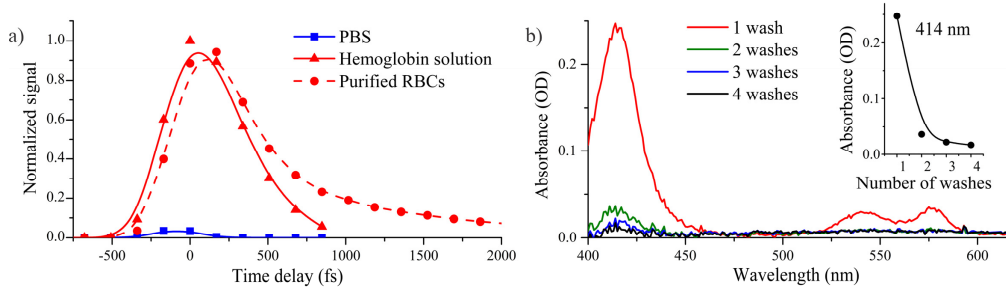


Fig. 9. a) Transient absorption measurements of PBS, hemoglobin solution and purified RBCs following 1040nm pump and 735nm probe. b) Absorption spectra of PBS solution with ghosts washed 1 to 4 times. Inset shows absorbance of ghosts after varying number of washes, probed at 414nm. Spectra were corrected for background and Rayleigh scattering.

4. Conclusion

We have investigated TPEF and THG for label-free non-invasive RBC imaging. Unlike conventional laser microscopy systems (>100 fs), the laser systems employed here produce very short pulses (15fs for the Ti:Sapphire and <45 fs for the Yb-fiber lasers). Therefore, these short-pulse sources deposit less thermal energy and reduce photo-thermal damage to the RBCs. TPEF signal increases as the inverse of pulse duration, while THG signals increase as the inverse of the pulse duration squared [35]. Following successful TPEF imaging of RBCs, we explored the source of the fluorescence and concluded it originated from two-photon excitation of the Soret band in hemoglobin based on fluorescence spectra, fluorescence lifetimes, as well as both linear and transient absorption data. The images are sufficiently detailed to assess morphological anomalies of RBCs non-destructively without breaching sterility using commercially available compact femtosecond laser oscillators.

Multi-photon microscopy modalities such as THG and TPEF can be used for non-invasive imaging of blood cells through the storage bag. Moreover, it was shown here that THG imaging provided the best resolution and image sensitivity for noninvasive imaging of stored RBCs without photodamage. We conclude that using compact and reliable ultrafast laser oscillators may lead to improvements in non-invasive blood analysis, including point-of-care assessment of RBC morphology.

Funding

Partial support for the MD group comes from NSF grant CHE-1464807. Support for the DS group comes from NIH grant EB016379. SO acknowledges the support of the Henry C. (1926) and Frances Keany Rickard Fund Fellowship via MIT.

Acknowledgments

We greatly appreciate Jayda Erkal and Kristen Entwistle from Spence Research Group for RBC sample preparation and handling. We also acknowledge Dr. Bai Nie, who built the Yb-fiber laser while a graduate student at Dantus Research Group. The Evans group also acknowledges Torrey Utne for his help in preparing blood samples.